PROCEEDINGS, 49th Workshop on Geothermal Reservoir Engineering
Stanford University, Stanford, California, February 12-14, 2024
SGP-TR-227

Mapping the Distribution of the Neutral Zone in Assist of Shallow Geothermal Applications in the United States

Rui MAO, Zilong ZHAO, Lei TIAN, Xinlei WANG, Ronaldo MAGHIRANG

Department of Agricultural and Biological Engineering, 1304 W. Pennsylvania Ave., University of Illinois at Urbana-Champaign, Urbana, IL 61801, USA

xwang2@illinois.edu (X. Wang)

Keywords: shallow geothermal energy, neutral zone, ground heat exchanger, parametric mapping

ABSTRACT

At depths of 5 to 20 meters below the ground surface, the geological stratum with stable temperature, known as the neutral zone, is crucial for climate battery and shallow geothermal applications. Currently, in the United States, very limited and fragmented data concerning the neutral zone, including its depth and temperature, primarily due to the prohibitive upfront costs associated with drilling tests. However, with the comprehensiveness of national meteorological and geophysical databases, the need for effective large-scale modeling of the shallow ground temperature has become feasible and urgent. This study introduces an analytical model established on the subsurface energy balance equations. By considering the conjugated heat flow at ground surface, solar radiation, and latent heat transfer, this model enables the anticipation of the temperature and depth of neutral zone based on the provided geological parameters. The simulation results were validated through a comparison against the soil temperature datasets at different depths in five documented case studies in Lemont and Argonne, IL; Houston, TX; Harrisburg, PA; and Teaneck, NJ. Two-dimensional thermal isopleths at various depths were generated across the United States, accompanied by the annual temperature fluctuations at neutral zone. This model enables early engineering assessments to identify potential climate battery candidate regions and facilitates the development of shallow geothermal applications through advancements in remote sensing technology and agricultural datasets.

1. INTRODUCTION

Unlike traditional energy sources that rely on burning fossil fuels, geothermal applications, harnessed from the heat stored beneath the Earth's surface, are increasingly adopted to mitigate the excessive carbon emissions in our current world (Alhuyi-Nazari et al., 2024; Abrasaldo et al., 2024; Zhao et al., 2023). Shallow geothermal energy, mainly referring to as the energy store within the depths up to 200 m, is particularly recognized as an alternative in field of space heating and cooling (Hamm et al., 2019; Sarbu and Sebarchievici, 2014; Zhao et al., 2022). Since the ground temperature found 10 ft beneath the ground surface is much more stable than the ambient air, the shallow geothermal applications provide inherent benefits such as high energy efficiency and reduced carbon footprints (Zhao et al., 2023). In recent years, studies related to the ground heat exchangers (GHEs) and ground source heat pump (GSHP) systems are conducted frequently. A black box heat pump model was developed to integrate the energy storage balance and control strategies (Weck-Ponten et al., 2022). The tool can be applied to plan shallow geothermal systems from a single building scale to a city district. The performance of thermosyphons utilized in extracting geothermal energy was investigated using a computational fluid dynamic method (Wang et al., 2020). The impacts of hydrostatic pressure on vaporization were analyzed and optimal filling quantity of working fluid for the thermosyphons were proposed. A stochastic design optimization model was developed to consider the random variation of geological parameters in the planned cost for a GSHP system (Zhao et al., 2021), where the results showed the economic benefits of higher groundwater velocity. The horizontal GHEs also attracted the efforts from many scholars. By introducing a novel device which is primarily composed of metal sheets, a box, a fin and the ground loop heat exchangers. By pouring the water into the device, the relatively humidity of the soil may be enhanced and thus improve the heat transfer efficiency of the GHE by 37% in one experimental scenario (Saeidi et al., 2022). A new coil-column system was proposed and tested with thermally enhanced grouting material (Kim et al., 2023). The new GHE showed three times higher in the heat exchange rate compared to the straight-line type GHE.

It is noticeable that in the studies related to the horizontal GHEs, one non-negligible characteristic is that the thermophysical properties of the geology are not as stable as compared to the deeper zone in the subsurface. In fact, for the near surface layer of the ground (usually referred to as the depth less than 40 cm), the ground temperature is actively fluctuating along with the environmental temperature above the ground surface. Then, approximately between the depths of 5 ~ 20 m, "neutral zone" is defined as the temperature of this zone can be regarded as constant throughout the year (Mao et al., 2023). Beneath the neutral zone, the slight gradient of temperature can be found over deeper subsurface. Progress can be found in recent research that has led to the development of models for predicting ground temperature and outlining temperature profiles at various depths. These soil profiles are determined using different methods: analytical methods, as demonstrated by Huang et al. (2020), empirical approaches as used by Droulia et al. (2009), and machine learning techniques as explored by Feng et al. (2019). Additionally, some research, such as that by Badache et al. (2016) and Ouzzane et al. (2015), employs polynomial fitting to represent the results, where the polynomial parameters effectively serve\ as factor weights. In many studies the correlation between air and soil temperatures is captured, often analyzed using Fourier analysis, as seen in works by Badache et al. (2016), Carson

(1963), Krarti et al. (1995), Lettau (1951), and Tong et al. (2021). Following this trend, some researchers, including Mihalakakou (2002) and Mihalakakou et al. (1997), have further improved this Fourier analysis approach by proposing their models.

Note that between the depths of 40 cm ~ 5 m, which can be called "buffer zone", there is a lack of knowledge on how to predict the temperature and its behaviors. However, most of the shallow geothermal applications are installed within this zone, which makes the lacked knowledge the key to optimize the design and operation of various geothermal applications. To accurately determine the thermal properties within the buffer zone, it is essential to thoroughly analyze the temperature at the neutral zone first. This analysis serves as a corner stone for deriving the temperature profiles of the geology at the buffer zone. Consequently, this study focuses on creating an analytical method to ascertain both the temperature and depth of the neutral zone in the United States.

2. FUNDAMENTALS OF THE PREDICTION MODEL

In this section, the mathematical model is introduced by following the documented mainstream studies that were using Fourier analysis to estimate the soil temperature profile in the assumption of unsteady heat conduction in a semi-infinite solid (Badache et al., 2016; Carslaw and Jaeger, 1986; Carson, 1963; Krarti et al., 1995; Kusuda,and Achenbach, 1965). To be more specific, the model designed for an annual cycle is employed to calculate the daily temperature at the neutral zone. For this purpose, the appropriate formulas are selected directly, and a detailed comparison of these choices can be found in the prior study (Mao et al., 2023).

2.1 Outline of the Prediction Model

Figure 1 depicts the structure of the mathematical model used in this study. The left graph exhibits different types of heat transfer and radiation considered in the model. The right workflow shows the sequence of the formulas being implemented. Energy Balance Equation (EBE) (Krarti et al., 1995), also known as Heat-Budget Equation at Ground Surface, is the fundamental equation to integrate all the factors as shown by Equation 1. In the equation, q_d and q_e represent short-wave and long-wave radiations from the sun and the environment, respectively; q_a and q_g symbolize the heat convection from the air and heat conduction from the deeper ground to the studied neutral zone. Additionally, q_w denotes the latent heat effect. The subsurface soil temperature profile, $T_{s(z,t)}$, is then formulated under the assumption that the soil domain is in a semi-infinite solid condition. And then it is used to derive the formulas of T_{sm}, T_{sv}, and ϕ_a. Once these values are determined, $T_{s(z,t)}$ effectively represents the temperature profile beneath the surface. The calculation details of the components in the model are presented below.

$$q_a + q_w + q_d + q_e + q_g = 0 \tag{1}$$

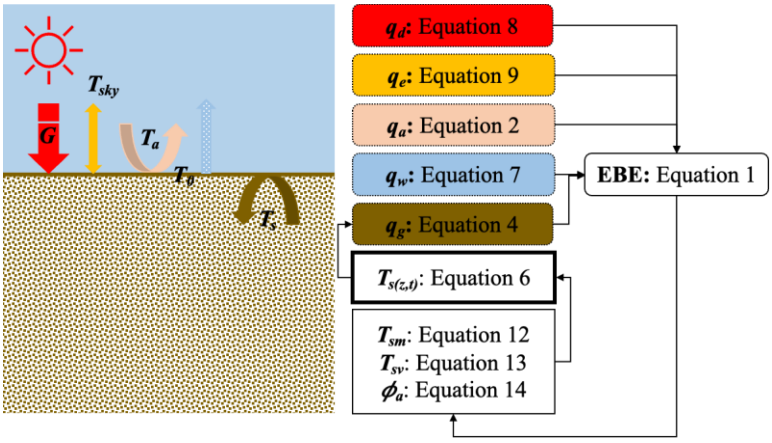

Figure 1: The demonstration of the energy balance modeling regarding the neutral zone.

2.2 Convection and Conduction

In a turbulent condition, the energy convection from air to the ground surface is evaluated based on their temperature difference (Hall and Allinson, 2010). Equation 2 gives the relationship between these parameters, where T_a denotes the air temperature and T_0 the ground surface temperature. As the temperature difference increases, the heat transfer rate from convection would also be increased.

$$q_a = h_a(T_a - T_0) \tag{2}$$

In the meantime, the convective heat transfer coefficient h_a can be regarded as a function of wind speed (Krarti et al., 1995; Lettau, 1951; Mihalakakou et al., 1997; Tong et al., 2021), which can be further elaborated depending on different scenarios. In our project, we use the formula improved by Tong et al., 2021, as presented through the Equation 3, where u is the wind speed, in m/s.

$$h_a(u) = \begin{cases} 5.7 + 3.8u^{0.5}, & u \le 4.88\ ms^{-1} \\ 7.2u^{0.78}, & u > 4.88\ ms^{-1} \end{cases} \tag{3}$$

On the other hand, the governing equation for heat conduction is given by Equation 4, where the value of heat transfer rate is determined by the soil thermal conductivity k_s and the temperature gradient along the depth z.

$$q_g = -(-k_s \frac{dT_o}{dz}) \tag{4}$$

In this case, the heat conduction at the ground surface is regarded as Equation 5.

$$\frac{dT_o}{dz} = \frac{\partial T_s(z,t)}{\partial z}\Big|_{z=0} \tag{5}$$

where, $T_{s(z,t)}$ represents the heat transfer in the subsurface, which is considered as transient heat conduction in a semi-infinite solid domain, as described in the works of Kusuda and Achenbach (1965), Carslaw and Jaeger (1986), and Carson (1963). Three key assumptions are made behind this theoretical formula: firstly, the influence from deep within the Earth is considered negligible; secondly, the average temperature remains constant at each depth; and thirdly, the amplitude diminishes as the depth increases. Therefore, $T_{s(z,t)}$ can be written as Equation 6.

$$T_s(z,t) = T_{sm} + T_{sv} e^{-\frac{z}{D}} \cos(wt - \frac{z}{D}) \tag{6}$$

where w denotes the time length of an observational period. T_{sm} the mean temperature during the period, T_{sv} the amplitude of temperature during the period, and D represents $\sqrt{2\alpha_s/w}$, where α_s denotes the soil diffusivity, in m^2/s.

2.3 Latent Heat Effect

In general, the latent heat effect due to the moisture (Primarily Water) includes evaporation, sublimation, melting, freezing, and condensation, while the evaporation process dominates in most cases. The empirical formula and parameters are given by Equation 4, which has been applied in most related studies (Badache et al., 2016; Krarti et al., 1995).

$$q_w = -cfh_a[(aT_0 + b) - r_a(aT_a + b)] \tag{7}$$

where, a, b and c are constant coefficients of which the values are 103 Pa/K, 609 Pa, and 0.0168 K/Pa, respectively. r_a denotes the relative humidity of air, and f is the evaporation coefficient, which mainly depends on the types of soil cover and the condition of soil moisture as indicated in Table 1.

Table 1: Evaporation coefficient under different soil conditions.

Soil moisture condition	Value of f
Dry soil	0
Arid soil	0.1 ~ 0.2
Moist soil	0.4 ~ 0.5
Wet soil	0.6 ~ 0.8
Saturated soil	1

2.4 Radiations

The radiation considered in this study includes the shortwave solar radiation, which is also known as insolation, and the longwave radiation emitted from the ambient environment. For the solar radiation, as Equation 5 depicts, β denotes the absorption coefficient, and G is the intensity of horizontal solar radiation, which is collected by meteorological stations. Note that the ground surface only absorbs a portion of it and for a fully illuminated ground surface, β can thus be calculated as $1 - albedo$ (Mihalakakou, 2002). When it comes to the longwave radiation, there are generally two methods to calculate it—a) a physical expression depending on the sky and the surface temperature (Badache et al., 2016; Król and Kupiec, 2019; Tong et al., 2021), and b) an empirical estimation shown by Equation 6 (Krarti et al., 1995).

$$q_d = \beta G \tag{8}$$

$$q_e = -\epsilon \Delta R \tag{9}$$

where ΔR represents a constant coefficient determined through experimental methods, which varies based on factors such as the radiative properties of the soil, the relative humidity of the ground and the air, and the effective sky temperature. A recommendation of an initial ΔR value is given as 63 W/m^2 (Krarti et al., 1995). Since the long-wave radiation is not a weighted factor, the empirical estimation is selected to be applied in our model and ΔR is set to be 100 W/m^2.

2.5 Air Temperature T_a and Intensity of Horizontal Solar Radiation G

There are two methods to achieve the direct fitting of periodic variation of T_a, and G observations--using complex function *exp(iwt)* (Badache et al., 2016; Krarti et al., 1995), and trigonometric function *cos(wt)* (Kusuda and Achenbach, 1965). The principles are similar and can be interchangeable. In this study the trigonometric function is selected, which is more compatible with Python programming environment and easier to be combined with the T_s formula as shown in Equation 10.

$$T_a = T_{am} + T_{av}\cos(wt + \phi_a) \tag{10}$$

where T_{am} denotes the mean air temperature during the certain time period, T_{av} the amplitude of the variation of air temperature, and ϕ_a the phase lag between the air and the soil.

To realize the regression to G, Equation 11 is applied.

$$G = G_m + G_v\cos(wt + \phi_G) \tag{11}$$

where G_m is the mean intensity of horizontal solar radiation during this period, and G_v is the amplitude of the intensity variation of horizontal solar radiation, and ϕ_G is the phase lag between the solar radiation and the soil.

2.6 Derivation of T_{sm}, T_{sv}, ϕ_h, and z_c

Given the equation deducing of EBE (Equation 1), the average temperature of soil, T_{sm}, the temperature amplitude at soil surface, T_{sv}, and the phase lag between air temperature and surface temperature, ϕ_h can be calculated based on the following equations (Equation 12, 13, and 14). Upon the results, the shallow subsurface soil temperature profile can be presented using Equation 6. T_{sm} can be regarded equivalent as T_c, that is, the temperature in the neutral zone.

$$T_{sm} = \frac{h_a(1+acfr_a)T_{am}+\beta G_m-\epsilon\Delta R+h_a bcf(r_a-1)}{h_a(1+acf)} \tag{12}$$

$$T_{sv} = \sqrt{\frac{[h_a(1+acfr_a)T_{am}]^2+(\beta G_m)^2+h_a(1+acfr_a)\cdot T_{am}\beta G_m\cdot\cos(\phi_{a-G})}{[h_a(1+acf)]^2+\frac{2k_S^2}{D^2}+2h_a(1+acf)\frac{k_S}{D}}} \tag{13}$$

$$\phi_a = \frac{\phi_{a-G}}{2}+\frac{\pi}{8}+\cos^{-1}\left(\frac{[h_a(1+acfr_a)T_{am}+\beta G_m]\cos\left(\frac{\phi_{a-G}}{2}\right)}{\sqrt{[h_a(1+acfr_a)T_{am}]^2+(\beta G_m)^2+h_a(1+acfr_a)\cdot T_{am}\beta G_m\cdot\cos(\phi_{a-G})}}\right)+\cos^{-1}\left(\frac{\left[h_a(1+acf)+\frac{\sqrt{2}k_S}{D}\right]\cos\left(\frac{\pi}{8}\right)}{\sqrt{[h_a(1+acf)]^2+\frac{2k_S^2}{D^2}+2h_a(1+acf)\frac{k_S}{D}}}\right) \tag{14}$$

3. MODEL SIMULATION AND VALIDATION

3.1 Input Data Preparation

In the US, the meteorological and soil data are prepared by remote sensing or collection of historical records as presented in Table 2. The meteorological datasets are obtained from the U.S. Climate Normals and National Solar Radiation Database (NSRDB) (Palecki et al., 2020; Sengupta et al., 2015), and the month global albedo map has been produced by NASA Earth Observation teams (Wan et al., 2015). The soil data used in the model are selected from the gridded National Soil Survey Geographic Database (gNATSGO), and then soil thermal diffusivity is derived based on the physical properties of soil, silt, and clay, such as soil bulk density, and water contents (Soil Survey Staff, 2020; Xie et al., 2018).

Table 2: Meteorological and soil data of contiguous U.S.

Dataset		Unit	Spatial Coverage	Spatial Resolution	Time Span	Temporal Resolution	Database	Reference
Meteorology	Ambient Temperature	*F*	National	1150 sites	2006-2020	Hourly	U.S. Climate Normals	Palecki et al., 2020
	Atmospheric Pressure	*hPa*						
	Wind Speed	*Mph*						
	Dew Point	*F*						
	Solar Radiation	$W\,m^{-2}$	National	1454 sites	1991-2005	Hourly	NSRDB	Sengupta et al., 2015
Soil	Surface Albedo	*DN*	World	0.1° × 0.1°	2000-2017	Monthly	NASA	Wan et al., 2015
	Soil Bulk Density	$g\,cm^3$	National		N/A	N/A	gNATSGO	

	Sand Content	% *W*		30 m × 30 m				Soil Survey Staff, 2020
	Silt Content	% *W*						
	Clay Content	% *W*						
	Water Content	% *W*						

3.2 Case Data Collection and Comparison

For the study of extremely shallow soil temperatures, there are relatively few records in the United States. The relevant studies are quite outdated, and the depths and chronological information tend to be fractured, random data, making it difficult to make comparisons (Reddy, 2000). After the systematic study conducted by Kusuda and Achenbach (1965) in 1965, the specific study was rarely continued until 2000 (Kusuda and Achenbach, 1965; Imadojemu, 1993; Reddy, 2000; Reddy and Imadojemu, 1995). Here, temperature records from five different locations in the US—Lemont and Argonne IL, Houston TX, Harrisburg PA, and Teaneck NJ have been collected as comprehensively as possible along the available years and depths, shown in Table 3. A direct comparison with the average annual temperature profile derived from the model can, to a certain extent, directly reflect the effectiveness of the average diagram.

Table 3: Information of records for comparison.

City, State	Geographic Coordinate	Time Span, year	Depth Coverage, m	Reference	Thermal Diffusivity, $*10^{-7}$ m^2 s^{-1}	Solar Radiation, W m^{-2}		Air Temperature, °C	
						Ave.	Amp.	Ave.	Amp.
Lemont, IL	41.67 °N, 87.99 °W	1952-1964	0.01-8.84	Kusuda, 1965	4.02	130.86	55.67	11.20	13.86
Argonne, IL	41.71 °N, 87.98 °W	1953-1955	0.01-8.84	Kusuda, 1965	4.02	130.86	55.67	11.20	13.86
Houston, TX	29.76 °N, 95.37 °W	1997-1998	0.00-5.79	Reddy, 2000	3.22	149.75	37.29	21.62	8.25
Harrisburg, PA	40.27 °N, 76.89 °W	1993?	0.00-6.10	Imadojemu, 1993	4.73	132.27	40.83	12.70	12.46
Teaneck, NJ	40.89 °N, 74.01 °W	1993?	1.52-4.57	Reddy and Imadojemu, 1995	2.94	136.05	36.45	13.01	12.47

The comparison between the model-generated temperature points and recorded data points has been made and presented by Figure 2 and Figure 3, regarding different depths. The solid curves represent the results obtained from the prediction model and the scatter points are plotted based on the database. It can be observed that the overall trends of the annual temperature align with each other. The predicted temperature values are generally slightly lower than the real data. This can be explained by the trivial heat dissipation that is neglected in the energy balance model. But in general, the regression R^2 for the comparison at the depth of 3 m is 0.89 while when it comes to deeper location, it is slightly improved to be 0.91, which shows sufficient accuracy of the proposed prediction method.

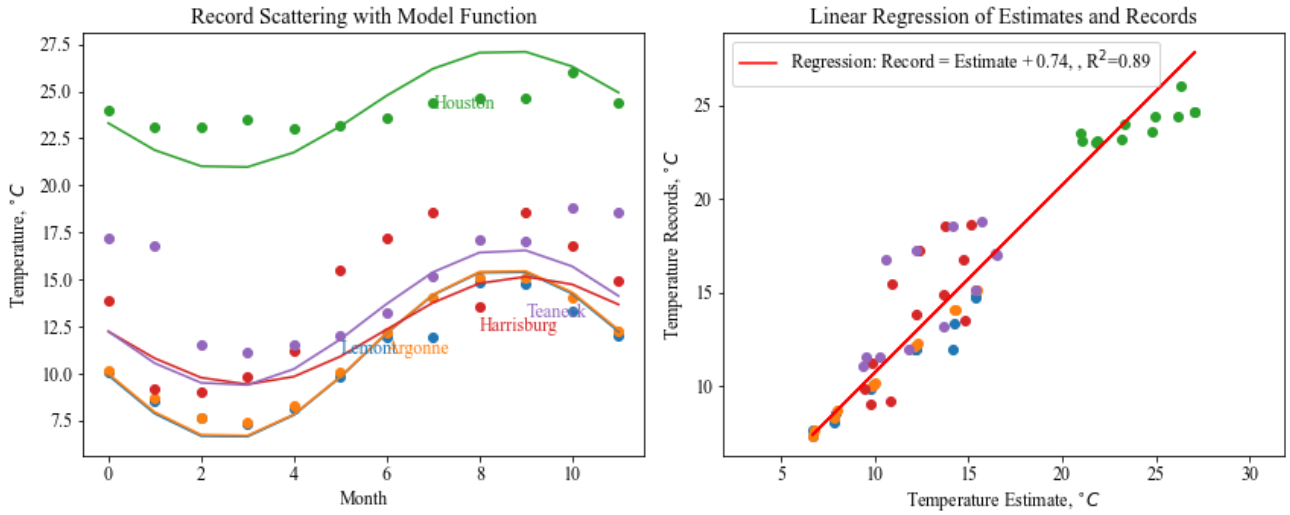

Figure 2: The comparison between the predicted annual temperature profile of soil and the temperature records from the database at 3 m-depth.

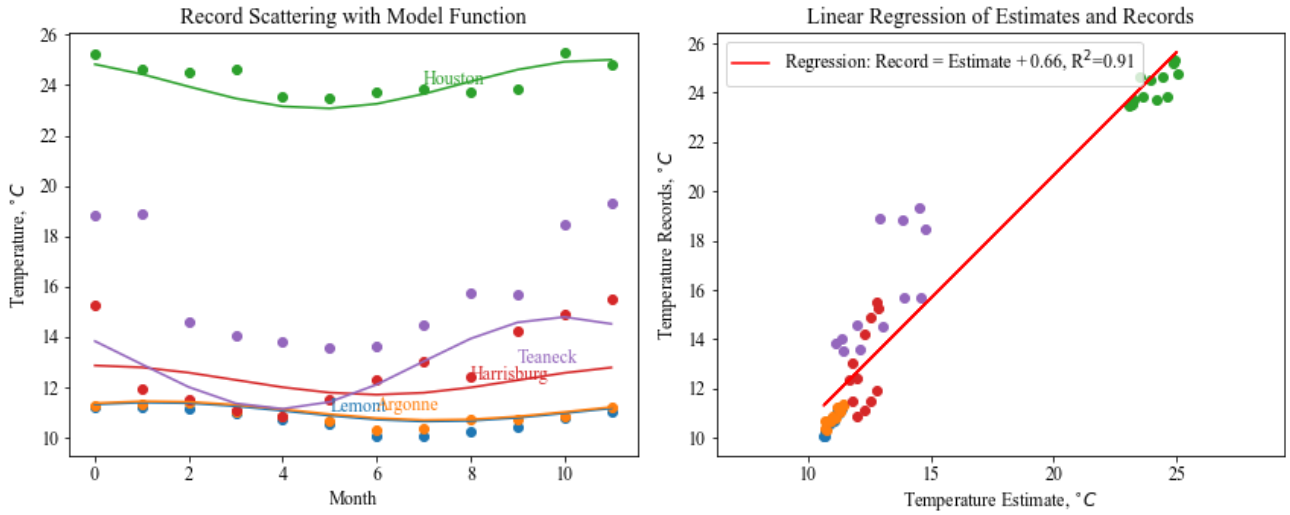

Figure 3: The comparison between the predicted annual temperature profile of soil and the temperature records from the database at deepest depths (deepest records from all the sites: 4.57-8.84, in general).

4. GEOTHERMAL MAPPING FOR NEUTRAL ZONE ACROSS THE US

4.1 Mapping of the Key Modeling Parameters across the US

The mapping for average temperature of soil (T_{sm}), average temperature of soil surface (T_{sv}), soil diffusivity (SD), air temperature yearly phase (ϕ_{air}), and phase lag between air and the soil (ϕ_h) across the United States have been presented by Figure 4. And to more explicitly show the trend of the data, the statistical analysis for the maps is provided in Table 4. The results show that the mean values of T_{sm} and T_{sv} are 16.21 ℃ and 15.72 ℃. If the entire dataset is approximated into a normal distribution, the standard deviation of the T_{sm} and T_{sv} are 5.78 ℃ and 2.88 ℃. The upper threshold for 90% of the data is 24.20 ℃ and 19.26 ℃, respectively. The values of SD, on the other hand, fall within a relatively smaller range—$5.10 \pm 1.09 \times 10^{-7}$ m^2/s across the country. Furthermore, the phase lag between air and soil ϕ_h is found within the range of -0.4 to 0.5 radius, as most of the data points fall within 0 ~ 0.12 radius.

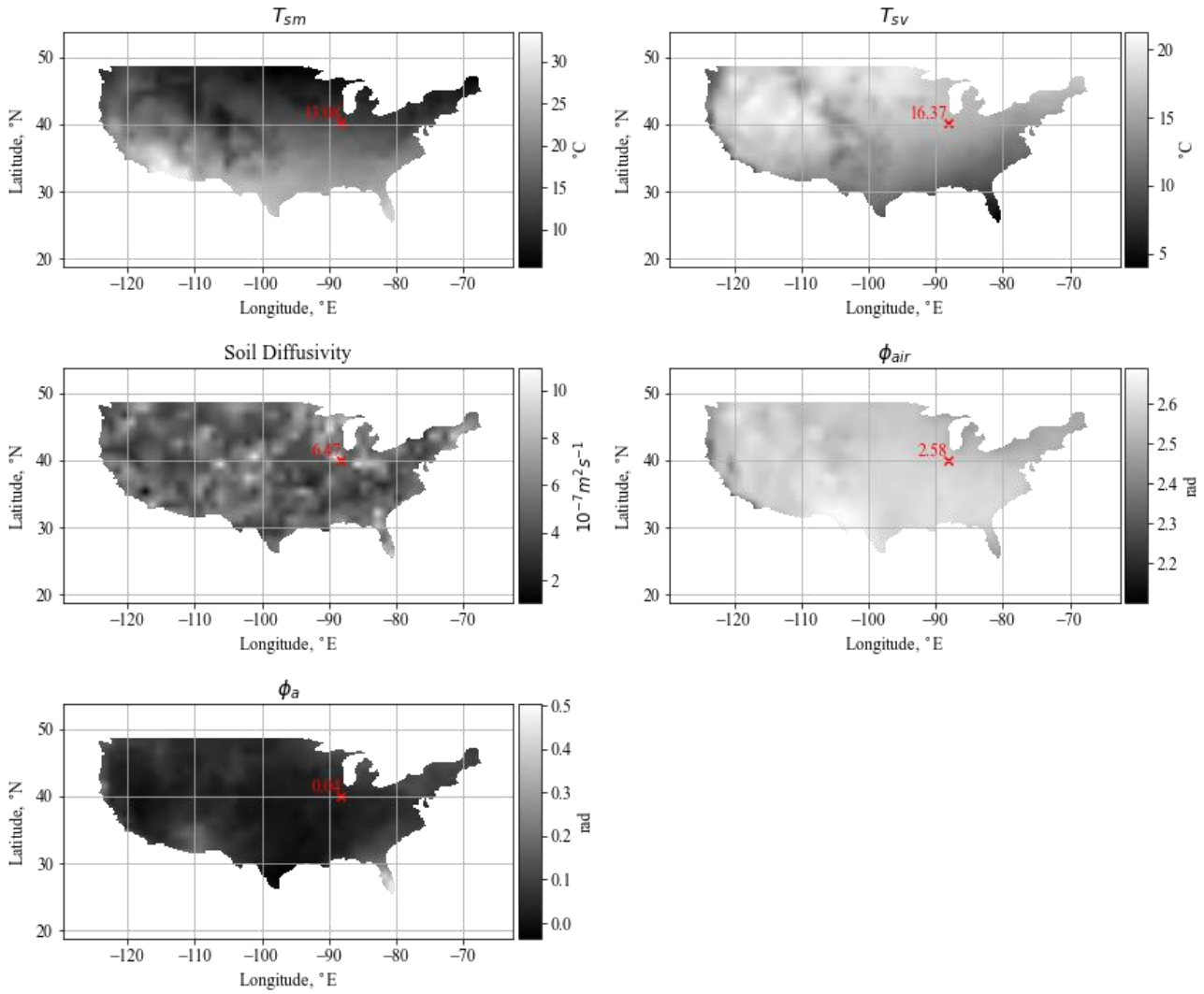

Figure 4: Maps of the key modeling parameters across the contiguous US with the example location mark (AESB UIUC).

Table 4: Statistical analysis for the key modeling parameters values across the contiguous US.

Variable	Unit	Average	Maximum	Minimum	Standard Deviation	Value not exceeded by 80% of the data	Value not exceeded by 90% of the data
T_{sm}	°C	16.21	33.53	5.55	5.78	21.82	24.20
T_{sv}	°C	15.72	21.29	4.04	2.88	18.31	19.26
SD	10^{-7} m^2/s	5.10	10.95	1.05	1.09	5.95	6.56
ϕ_{air}	radius	2.57	2.69	2.10	0.05	2.61	2.62
ϕ_a	radius	0.06	0.50	-0.4	0.05	0.09	0.12

To better demonstrate the relationship between the annual soil temperature profile and the depth, a specific location in central Illinois—Champaign, is selected to show the local thermal environment in the subsurface. Figure 5: Soil Profile Example (AESB UIUC). shows both the soil temperature contour over time in a year and the amplitude of the temperature variation over various depths at the Agricultural Engineering Sciences Building (AESB) at the University of Illinois at Urbana-Champaign (UIUC). It is noticeable that the near-surface region exhibits more season-dependent characteristics. For instance, at the depth of 2 m, the maximum annual fluctuation of soil temperature may reach near 15 ℃, while at depths over 10 m, the amplitude becomes less than 1 ℃.

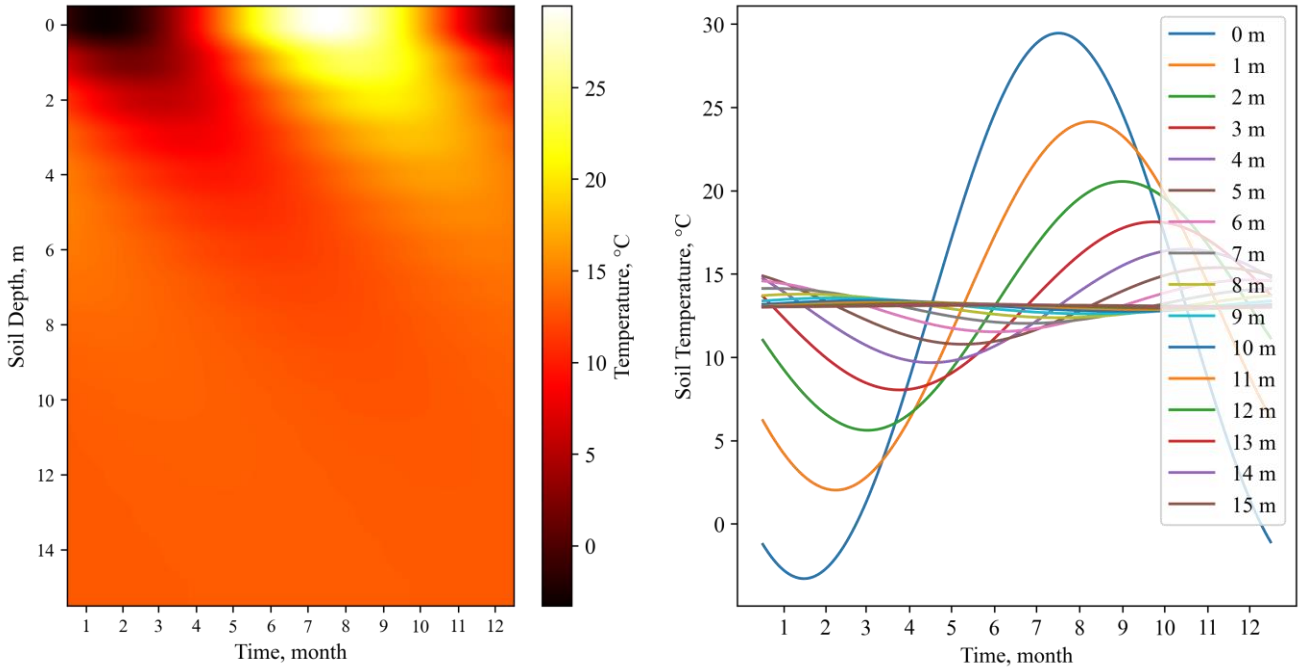

Figure 5: Soil Profile Example (AESB UIUC).

4.2 Simple Relationships between the Mean Soil Temperature (T_{sm}), Mean Air Temperature (T_{sv}) and Other Key Parameters

Based on the data points computed by the prediction model, a simplified, estimated relation between the T_{sm} and T_{sv} are obtained as below. With a $R^2 = 0.86$, the mean soil temperature can be correlated by a linear, monotonically changing function with the variation of mean air temperature.

$$T_{sm} = 1.11T_{am} + 1.73, R^2 = 0.86 \quad (15)$$

In the meantime, to provide a fast estimation approach, using the database that includes the latitudes, longitudes, and the output mean soil temperature, a reasonably good correlation between them is shown by Equation 18. This can be used in general engineering applications where limited data is accessible and a rough estimation of soil temperature is desired.

$$T_{sm} = -1.00L + 0.00018A + 55.16, R^2 = 0.81 \quad (16)$$

where, L is latitude in °N, and A is altitude in m.

Furthermore, the variation trend of the standard deviations regarding the amplitude of the T_{sm} profile and the varied depths is generated and shown by Figure 6. As expected, the fluctuation magnitude of the soil temperature decreases as the depth goes deeper. At the ground surface, which is depth of 0 m, the amplitude exhibits the same as that of the ambient air temperature. However, when it comes to the depth of around 10 m, the amplitude is reduced to approximately 0.39 ℃, with a 90% confidence less than 0.67 ℃ for all locations. Therefore, it can be safely concluded that in the contiguous US, the soil temperature at the depth of 10 meters tends to remain constant, with an average year-round variation < 1 °C. The stable annual soil temperature can thus have this depth be regarded as the general boundary of the neutral zone in the contiguous US.

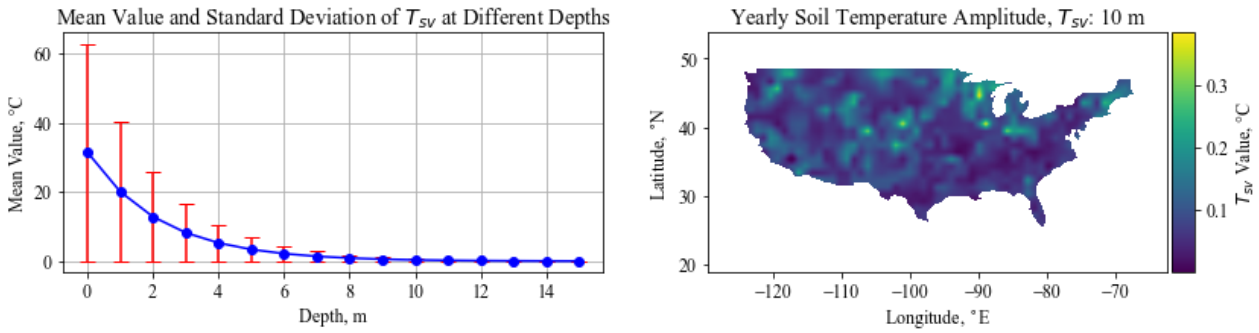

Figure 6: The variation of the T_{sv} profile along the depths and T_{sv} contour at the depth of 10 m in the contiguous US.

5. DISCUSSION AND CONCLUSION

This study aims at deriving datasets for the neutral zone (constant temperature ground layer) and its application in mapping shallow soil temperatures in the United States. The derivation of this shallow data utilizes daily average values; however, this model does not fully capture daily variations due to its inability to represent daily radiation changes with standard trigonometric functions. Furthermore, daily variations in shallow layers are significantly influenced by various factors such as sunlight penetration from top to bottom, air convection, and heat conduction in the soil, moving both upwards and sideways. Thus, to analyze these daily variations, a more sophisticated model of unsteady heat conduction is required, for which this research provides foundational data and boundary conditions. The focus of this study is the contiguous United States, and it yields several key findings:

a) The comprehensive mapping for key parameters including average soil temperature (T_{sm}), average temperature of soil surface (T_{sv}), soil diffusivity (SD), and phase lag of air (ϕ_a) across the United States are generated using geographical factors including latitude and altitude, without the need for meteorological data.
b) Fast estimation correlations between the mean soil temperature (T_{sm}) and mean air temperature (T_{sv}), mean soil temperature (T_{sm}) and the coordinates of the location, amplitude of T_{sm} and the depth in the subsurface are obtained from the prediction model, which can be applied to various engineering scenarios where basic geothermal information is required but with limited testing records or data accessibility.
c) The depth (upper boundary) of the neutral zone can be roughly estimated from this study, which is approximately 10 m. This can be useful in geothermal applications such as GSHP or earth shelter in agricultural applications, accompanied by a detailed soil temperature variation profile along the depth.

The future studies may consider incorporating the soil temperature profile into building load profiles for co-simulation purposes on more advanced geothermal applications.

REFERENCES

Alhuyi-Nazari, M., Mukhtar, A., Yasir, A. S. H. M., Ahmadi, M. H., Kumar, R., and Luong, T.: Applications of geothermal sources for absorption chillers as efficient and clean cooling technologies for buildings: A comprehensive review, Journal of Building Engineering, 82, (2024), 108340.

Abrasaldo, P. M. B., Zarrouk, S. J., and Kempa-Liehr, A. W.: A systematic review of data analytics applications in above-ground geothermal energy operations, Renewable and Sustainable Energy Reviews, 189, (2024), 113998.

Badache, M., Eslami-Nejad, P., Ouzzane, M., Aidoun, Z., and Lamarche, L.: A New Modeling Approach for Improved Ground Temperature Profile Determination, Renewable Energy, 85, (2016), 436-444.

Carslaw, H.S., and Jaeger, J.C.: Conduction of heat in solids, 2nd ed. Oxford University Press, London, England, (1986).

Carson, J. E.: Analysis of Soil and Air Temperatures by Fourier Techniques, Journal of Geophysical Research, 68, 8, (1963), 2217-2232.

Droulia, F., Lykoudis, S., Tsiros, I., Alvertos, N., Akylas, E., and Garofalakis, I.: Ground temperature estimations using simplified analytical and semi-empirical approaches, Solar Energy, 83(2), (2009), 211-219.

Feng, Y., Cui, N., Hao, W., Gao, L., and Gong, D.: Estimation of soil temperature from meteorological data using different machine learning models, Geoderma, 338, (2019), 67-77.

Hall, M.R., and Allinson, D.: 1 - Heat and Mass Transport Processes in Building Materials, Editor(s): Matthew R. Hall, In Woodhead Publishing Series in Energy, Materials for Energy Efficiency and Thermal Comfort in Buildings, Woodhead Publishing, (2010), 3-53.

Huang, R., Huang, J.-X., Zhang, C., Ma, H.-Y., Zhuo, W., Chen, Y.-Y., and Mansaray, L. R.: Soil temperature estimation at different depths, using remotely sensed data. Journal of Integrative Agriculture, 19, (2020), 277–290.

Hamm, S.G., Augustine, C. R., Tasca, C., and Winick, J.: An Overview of the U.S. Department of Energy's GeoVision Report, GRC Transactions, 43, (2019).

Imadojemu, H. E.: Earth's Temperature Variation with Depth, American Society of Mechanical Engineers (Paper), Proceedings of the ASME Winter Conference, (1993), 1-8.

Kim, Y., Dinh, H., Kang, G., and Hoang, D.: Performance evaluation of a novel horizontal ground heat exchanger: Coil-column system, Journal of Building Engineering, 76, (2023), 107180.

Król, B., and Kupiec, K.: Study of Temperature Distribution in the Ground, Chemical and Process Engineering - Inzynieria Chemiczna i Procesowa, 40, (2019), 123-137.

Krarti, M., Lopez-Alonzo, C., Claridge, D. E., and Kreider, J. F.: Analytical Model to Predict Annual Soil Surface Temperature Variation, ASME. J. Sol. Energy Eng, 117, 2, (1995), 91–99.

Kusuda, T., and Achenbach, P.R.: Earth Temperature and Thermal Diffusivity at Selected Stations in the United States, (1965).

Lettau, H.: Theory of Surface-Temperature and Heat-Transfer Oscillations near a Level Ground Surface, Eos Trans. AGU, 32, 2, (1951), 189–200.

Mao, R., Zhao, Z., Tian, L., Fang, T., and Wang, X.: Generation of Gridded Temperature Map of Constant-Temperature Layer Based on Meteorological Data for Shallow Geothermal Applications, Geothermics, 113, (2023), 102770.

Mihalakakou, G.: On Estimating Soil Surface Temperature Profiles, Energy and Buildings, 34, 3, (2002), 251-259.

Mihalakakou, G., Santamouris, M., Lewis, J. O., and Asimakopoulos, D. N.: On the application of the energy balance equation to predict ground temperature profiles. Solar Energy, 60, (1997), 181-190.

Ouzzane, M., Eslami-Nejad, P., Badache, M., and Aidoun, Z.: New correlations for the prediction of the undisturbed ground temperature, Geothermics, 53, (2015), 379-384.

Palecki, M., Durre I., Applequist, S., Arguez, A., and Lawrimore, J.: U.S. Climate Normals 2020: U.S. Hourly Climate Normals (2006-2020), NOAA National Centers for Environmental Information, (2020).

Reddy, G. B.: An Experimental Investigation of Subsurface Ground Temperature in Texas: A Complete Study, International Journal of Ambient Energy, 21:4, (2000), 196-202.

Reddy, G. B., and Imadojemu, H. E.: A Study of Subsurface Ground Temperatures at Selected Locations in the United States, International Journal of Ambient Energy, 16:1, (1995), 23-32.

Sengupta, M., Weekley, A., Habte, A., Lopez, A., and Molling, C.V.: Validation of the National Solar Radiation Database (NSRDB) (2005-2012): Preprint, European PV Solar Energy Conference and Exhibition, 9, (2015).

Saeidi, R., Karimi, A., and Noorollahi, Y.: The novel designs for increasing heat transfer in ground heat exchangers to improve geothermal heat pump efficiency, 116, (2024), 102844.

Soil Survey Staff: Gridded National Soil Survey Geographic (gNATSGO) Database for the Conterminous United States. United States Department of Agriculture, Natural Resources Conservation Service, 8, 9, (2020).

Sarbu, I. and Sebarchievici, C.: General review of ground-source heat pump systems for heating and cooling of buildings, Energy and Buildings, 70, (2014), 441-454.

Tong, C., Li, X., Duanmu, L., and Wang, H.: Prediction of the Temperature Profiles for Shallow Ground in Cold Region and Cold Winter Hot Summer Region of China, Energy and Buildings, 242, (2021), 110946.

Wan, Z., Hook, S., and Hulley, G.: MOD11C3 MODIS/Terra Land Surface Temperature/Emissivity Monthly L3 Global 0.05Deg CMG V006 [Data set]. NASA EOSDIS Land Processes Distributed Active Archive Center, (2015).

Wang, X., Liu, H., Wang, Y., and Zhu, Y.: CFD simulation of dynamic heat transfer behaviors in super-long thermosyphons for shallow geothermal application, Applied Thermal Engineering, 174, (2020), 115295.

Weck-Ponten, S., Frisch, J., and Treeck, C.: Simplified heat pump system model integrated in a tool chain for digitally and simulation-based planning shallow geothermal systems, Geothermics, 106, (2022), 102579.

Xie, X., Lu, Y., Ren, T., and Horton, R.: An Empirical Model for Estimating Soil Thermal Diffusivity from Texture, Bulk Density, and Degree of Saturation. Journal of Hydrometeorology, 19, 2, (2018), 445 – 457.

Zhao, Z., Lin, Y., Stumpf, A., and Wang, X.: Assessing impacts of groundwater on geothermal heat exchangers: A review of methodology and modeling, Renewable Energy, 190, (2022), 121-147.

Zhao, Z., Lin, Y., Stumpf, A., and Wang, X.: Improving LEED-certified building loads on borehole heat exchangers by coupling subsurface variables, Applied Thermal Engineering, 224, (2023), 120119.

Zhao, Z., Stumpf, A., Lin, Y., and Wang, X.: Impacts of prospective LEED building's energy loads on a borehole heat exchanger: A case study in Central Illinois, Proceedings of the IGSHPA Research Track, (2022).

Zhao, Z., Xu, Y., Lin, Y., Wang, X., and Wang, P.: Probabilistic modeling and reliability-based design optimization of a ground source heat pump system, Applied Thermal Engineering, 197, (2021), 117341.

APPENDIX: SOIL TEMPERATURE RECORDS IN DIFFERENT CITIES FROM DOCUMENTED STUDIES.

City	**Lemont, IL**											
Depth, m	Monthly Average Temperature, C											
	Jan	Feb	Mar	Apr	May	Jun	Jul	Aug	Sep	Oct	Nov	Dec
0.01	-0.44	0.44	3.22	9.39	15.50	23.00	24.56	23.94	19.17	14.11	5.67	1.00
0.10	-0.39	0.22	2.67	8.61	14.83	22.72	24.33	23.72	18.83	14.00	6.28	1.11
0.20	0.22	0.44	2.67	8.00	13.94	21.33	23.44	23.00	18.94	14.56	7.22	2.00
0.50	1.78	1.56	2.89	7.11	12.22	18.67	21.44	21.67	19.06	15.33	9.22	4.11
1.00	4.33	3.22	3.72	6.33	10.33	15.44	18.72	19.78	18.78	15.89	11.11	6.89
3.05	10.11	8.56	7.67	7.33	8.11	9.83	11.94	11.94	14.83	14.78	13.33	12.00
8.84	11.22	11.22	11.17	11.00	10.72	10.56	10.06	10.06	10.28	10.44	10.78	11.06
City	**Argonne, IL**											
Depth, m	Monthly Average Temperature, C											
	Jan	Feb	Mar	Apr	May	Jun	Jul	Aug	Sep	Oct	Nov	Dec
0.01	-4.44	-1.50	0.89	9.67	14.11	20.50	23.11	21.83	17.83	11.78	3.11	-3.11
0.10	-0.17	0.28	3.11	10.06	15.94	22.22	25.56	24.44	19.56	13.61	5.89	0.94
0.20	-0.11	0.06	2.50	9.39	15.39	21.83	25.06	24.00	19.22	13.56	5.83	0.89
0.50	0.50	0.28	2.44	8.78	14.50	20.67	24.00	23.39	19.33	14.06	6.78	1.67
1.00	2.11	1.39	2.78	7.61	12.78	18.22	21.61	22.00	19.28	15.06	8.83	3.83
3.05	4.44	3.28	3.67	6.61	10.89	15.28	18.83	20.06	18.89	15.89	11.22	6.94
8.84	10.17	8.72	7.67	7.39	8.33	10.06	12.17	14.06	15.11	15.11	14.06	12.28
City	Houston, TX											
Depth, m	Monthly Average Temperature, C											
	Jan	Feb	Mar	Apr	May	Jun	Jul	Aug	Sep	Oct	Nov	Dec
0.00	19.67	19.76	21.70	25.99	29.28	30.19	31.55	32.72	31.23	27.69	21.71	18.43
0.30	19.91	20.47	21.86	25.51	28.33	29.18	30.06	31.43	30.62	27.86	23.20	20.12
0.61	20.64	20.59	21.61	24.81	26.76	28.34	29.08	30.39	29.92	27.60	23.87	20.84
0.91	21.06	20.80	21.58	24.27	25.78	27.02	27.60	28.62	28.40	26.58	24.44	21.46
1.22	21.43	21.08	21.65	23.95	25.24	26.61	27.33	28.18	28.11	26.54	24.77	21.97
1.52	21.88	21.36	21.78	23.61	24.23	25.28	26.18	27.21	27.28	26.22	25.20	22.57
1.83	22.34	21.65	21.96	23.50	23.81	24.81	25.76	26.83	27.04	26.25	25.53	23.08
2.13	22.87	22.05	22.19	23.44	23.52	24.49	25.41	26.46	26.76	26.26	25.80	23.55
2.44	23.36	22.39	22.48	23.41	23.32	23.99	24.77	25.78	26.07	25.79	25.97	23.93
2.74	23.36	22.69	22.49	23.41	23.64	23.69	24.31	25.20	25.51	25.31	25.99	23.99
3.05	23.98	23.12	23.10	23.51	23.03	23.14	23.61	24.43	24.64	24.63	26.02	24.37
3.35	24.12	23.34	23.29	23.64	23.04	23.24	23.95	24.70	24.91	24.78	25.99	24.52
3.66	24.14	23.44	23.33	23.64	23.37	23.21	23.90	24.58	24.78	24.89	25.98	24.57
3.96	24.14	23.51	23.33	23.64	23.37	23.26	24.01	24.74	24.92	25.09	25.95	24.59
4.27	24.52	23.77	23.62	23.88	22.91	23.07	23.98	24.46	24.47	24.65	25.59	24.71
4.57	24.79	24.03	23.88	24.06	23.23	23.03	23.66	24.13	24.18	24.37	25.49	24.80

4.88	25.06	24.37	24.23	24.34	23.37	23.05	23.36	23.80	23.78	23.93	25.54	24.99
5.18	25.08	24.41	24.26	24.35	23.47	23.37	23.66	23.84	23.83	23.96	25.42	24.97
5.49	25.13	24.52	24.34	24.51	23.46	23.38	23.72	23.89	23.79	23.89	25.38	24.93
5.79	25.21	24.64	24.50	24.66	23.54	23.49	23.73	23.86	23.75	23.87	25.32	24.79
City	**Harrisburg, PA**											
Depth, m	Monthly Average Temperature, C											
	Jan	Feb	Mar	Apr	May	Jun	Jul	Aug	Sep	Oct	Nov	Dec
0.00	16.17	1.33	5.50	10.78	17.39	25.17	29.89	24.83	16.28	15.72	15.94	16.17
0.15	6.72	2.44	5.56	10.50	16.61	23.50	26.44	23.89	13.67	15.78	11.50	7.17
0.30	6.94	2.89	5.56	10.44	16.00	22.72	26.00	23.89	13.67	16.33	12.06	7.72
0.46	7.33	3.33	5.67	10.28	15.67	22.39	25.61	23.72	13.67	16.78	12.50	8.17
0.61	7.78	3.67	5.78	10.22	15.22	22.00	25.06	23.67	13.72	17.28	13.06	8.78
0.76	8.22	4.17	6.00	10.11	14.83	21.61	24.50	23.56	13.83	17.72	13.61	9.44
0.91	8.83	4.67	6.33	10.11	14.50	21.22	23.83	23.28	13.89	18.11	14.17	10.17
1.22	9.78	5.56	6.67	9.89	13.56	20.22	22.56	22.83	13.89	18.67	15.00	11.33
1.52	10.67	6.28	7.00	9.67	12.89	19.39	21.50	22.11	13.83	19.00	15.61	12.28
1.83	11.39	6.89	7.39	9.61	12.39	18.61	20.61	21.50	13.83	19.22	16.06	12.89
2.13	12.11	7.61	7.83	9.61	11.72	17.72	19.72	20.83	13.72	19.22	16.39	13.50
2.44	12.78	8.22	8.17	9.61	11.61	16.94	18.78	20.06	13.67	19.11	16.61	14.06
2.74	13.33	8.67	8.56	9.72	11.39	16.17	17.94	19.28	13.56	18.83	16.67	14.50
3.05	13.89	9.22	9.06	9.83	11.22	15.50	17.22	18.56	13.56	18.61	16.78	14.94
3.35	14.39	9.72	9.39	10.00	11.11	14.78	16.44	17.72	13.44	18.22	16.78	15.28
3.66	14.78	10.33	9.94	10.17	11.06	14.22	15.72	17.06	13.39	17.83	16.72	15.61
3.96	15.17	10.83	10.50	10.50	11.17	13.78	15.28	16.50	13.44	17.50	16.72	15.89
4.27	15.28	11.17	10.72	10.56	11.00	13.28	14.61	15.78	13.28	16.94	16.39	15.89
4.57	15.33	11.39	10.94	10.67	10.94	12.78	14.06	15.11	13.06	16.33	16.11	15.83
4.88	15.44	11.61	11.17	10.83	11.00	12.44	13.67	14.67	13.00	15.89	15.94	15.94
5.18	15.44	11.78	11.33	10.94	11.00	12.17	13.22	14.17	12.83	15.44	15.61	15.78
5.49	15.39	11.89	11.50	11.11	11.06	11.89	12.94	13.72	12.72	15.00	15.33	15.67
5.79	15.33	12.06	11.50	11.11	11.00	11.67	12.67	13.39	12.61	14.56	15.06	15.61
6.10	15.28	11.94	11.50	11.11	10.89	11.50	12.33	13.06	12.44	14.22	14.89	15.50
City	**Teaneck, NJ**											
Depth, m	Monthly Average Temperature, C											
	Jan	Feb	Mar	Apr	May	Jun	Jul	Aug	Sep	Oct	Nov	Dec
1.52	12.89	12.56	5.61	7.89	10.44	14.33	17.61	20.72	20.78	17.72	17.06	15.17
3.05	17.22	16.78	11.56	11.11	11.56	12.00	13.22	15.17	17.11	17.00	18.83	18.56
4.57	18.83	18.89	14.61	14.06	13.83	13.56	13.61	14.50	15.72	15.67	18.44	19.33